Spreading of Normal Liquid Helium Drops

David Mallin,[1] Kenneth R. Langley,[2] Andres A. Aguirre-Pablo,[2] Matthew L. Wallace,[1] Michael Milgie,[1] Sigurdur T. Thoroddsen,[2] and Peter Taborek[1]

[1]*Department of Physics and Astronomy, University of California Irvine, Irvine, California 92697, USA*

[2]*Division of Physical Sciences and Engineering, King Abdullah University of Science and Technology (KAUST), Thuwal 23955-6900, Saudi Arabia*

(Received 9 July 2020; accepted 1 October 2020; published 21 October 2020)

We have used video imaging and interferometric techniques to investigate the dynamics of spreading of drops of ^{4}He on a solid surface for temperatures ranging from 5.2 K (near the critical point) to 2.2 K (near T_λ). After an initial transient, the drops become pancake-shaped with a radius that grows as $R(t) \approx t^\alpha$, with $\alpha = 0.149 \pm 0.002$. The drops eventually begin to shrink due to evaporation driven by gravitational and curvature effects, which limits their lifetime to about 1000 s. Although helium completely wets the substrate, and the spreading takes place over a pre-existing adsorbed film, a distinct contact line with a contact angle of order one degree is visible throughout this process.

DOI: 10.1103/PhysRevE.102.043105

I. INTRODUCTION

When a drop of fluid is deposited on a solid surface, surface tension and gravitational forces will cause it to spread. If the fluid partially wets the solid, then the drop will come to equilibrium with a contact angle θ_c given by the Young equation $\cos(\theta_c) = (\sigma_{sv} - \sigma_{sl})/\sigma_{lv}$ where σ_{sv}, σ_{sl}, and σ_{lv} are the solid-vapor, solid-liquid, and liquid-vapor interfacial energies, respectively. If the characteristic size of the drop is small compared to the capillary length $L_c = \sqrt{\sigma_{lv}/(g\rho)}$, where g is the acceleration due to gravity and ρ is the fluid mass density, then the drop assumes a spherical cap shape which minimizes the surface energy; while if the characteristic size is greater than L_c, then gravitational energy dominates and the drop evolves into a pancake shape [1].

In contrast, if the fluid completely wets the substrate (i.e., if $\sigma_{lv} < \sigma_{sv} - \sigma_{sl}$), then the drop will eventually spread into a molecularly thin flat film. Because of its importance in coating technologies, the kinetics of the spreading process has been extensively studied both theoretically [2,3] and experimentally [4–6]. Much of the experimental work has utilized silicone oil as the working fluid. Even if the fluid completely wets the substrate and the equilibrium contact angle is zero, during the spreading process there is a well-defined advancing contact line and contact angle. Experiments using conventional fluids show that the drop spreading footprint radius $R(t)$ typically grows as a power of time t, $R(t) \sim t^\alpha$, with $0.1 < \alpha < 0.15$, and with a prefactor which depends on the fluid viscosity. One common theoretical approach is to model the fluid flow in the drop using the hydrodynamic lubrication approximation, which quantitatively balances surface tension and gravitational forces against viscous forces with the additional constraint of volume conservation. For axisymmetric spherical cap drops driven by surface tension forces, a well-known asymptotic solution often called Tanner's law [7] yields $R(t) \sim t^{1/10}$. The spherical cap approximation is only valid for drops with characteristic size less than the capillary length. For larger drops, gravity dominates surface tension forces, and for this case of gravity driven spreading, the lubrication approximation yields [8,9] $R(t) \sim t^{1/8}$.

Another approach to contact line dynamics focuses attention on dissipative processes at the contact line rather than viscous dissipation in the bulk flow. This molecular kinetic theory (MKT) models contact line motion as a sequence of thermally activated steps in a washboard potential that describes the driving force for spreading and pinning forces at the substrate. For a spherical cap drop driven by surface tension [10–12], the MKT asymptotic dynamics are $R(t) \sim t^{1/7}$, but pancake drop geometries or gravitational driving forces yield different exponents. It is important to note that the value of the exponents is independent of the magnitude of the dissipation, which only appears as a prefactor to the power law. A simplified discussion of these spreading laws and the crossover regimes between the various power laws is discussed in the Appendix.

There are several motivations for studying spreading of liquid helium. Helium has a very low surface tension and wets all substrates except cesium [13–15]. Even in the normal state, the viscosity is approximately a million times lower than silicone oils. (Spreading in the superfluid state is quite unusual and is discussed in a separate recent publication [16].) Liquid heluim has some unusual properties (at a temperature of 2.5 K, Helium has a density ρ of 144.8 kg/m^3, a surface tension σ of 262.3 μN/m, and a dynamic viscosity η of 3.259×10^{-13}kg/m $*$ s). Conventional room temperature spreading experiments usually take place in air, and the spreading drop advances into a dry region with a possible precursor film [17] that advances ahead of the three phase contact line. The helium experiments, in contrast, are done at the saturated vapor pressure, so the drop advances into a "moist" region covered by a liquid film of typical thickness 40 nm which is stabilized by the van der Waals interaction

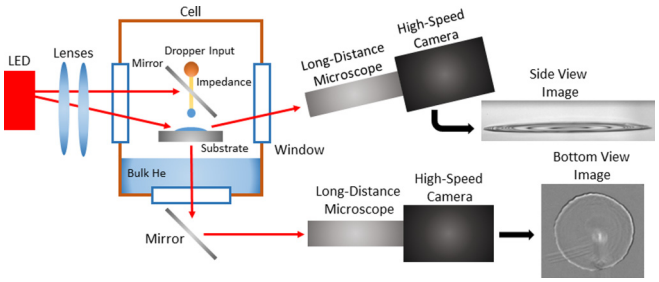

FIG. 1. Schematic diagram of cryogenic and optical apparatus. Drops were delivered from a capillary tube approximately 1 cm above the substrate, which was usually a sapphire plate. The spreading drop was illuminated with collimated and filtered LED light, which was shone at a shallow angle for the edge-on view, or reflected from a 45 degree mirror to produce normal incident light for the bottom view. The level of the bulk liquid in the cell was approximately 1 cm below the top of the substrate.

with the solid substrate. We find that the most appropriate model for the conditions of our experiment is surface tension driven spreading of a pancake-shaped drop which corresponds to a spreading exponent of 1/7.

II. EXPERIMENT

The cryogenic and optical setup of our apparatus is shown in Fig. 1. The experimental cell was housed in a continuous pulse tube/^{4}He evaporation cryostat with multiple optical access ports. An optical grade sapphire substrate or quartz crystal microbalance (QCM) was mounted within the cell as the impacting surface. A dropper was mounted above the sapphire through a metallic mirror positioned at a 45° angle. All experiments were performed with bulk liquid at the bottom of the experimental cell, ensuring a saturated vapor environment. Helium drops were produced by increasing the pressure in the dropper line sufficiently above the cell vapor pressure for the given temperature. A 5 μm ID tube in the dropper line acts as a flow impedance to limit the drop rate from once every 2 min to once every 20 min. Because the pressure in the cell is always at the saturated vapor pressure, the substrate was covered in a thin film of liquid helium even before the drop impacts. The film thickness was measured to be 12–40 nm by the QCM.

An LED was used in pulsed mode to minimize heat input in the cell due to the light. The light from the LED traveled through a series of collimating lenses limiting illumination to the area of interest, with a bandpass filter for performing interferometry on the drops. The camera was mounted opposite and pointing toward the LED to form a side view image in reflected light, or mirrors were used to form a bottom view image in transmitted light. In the side-view configuration, the LED source and camera were tilted downward at an angle of 6.4°. In the bottom view configuration, the LED and the camera were horizontal and an additional mirror outside the cryostat was used to reorient the image.

In the side view, the camera is tilted at a 6.4° angle, allowing interference fringes to be imaged, as seen in Fig. 2. The drops are sufficiently flat that they locally can be described as a thin liquid film with change in film thickness

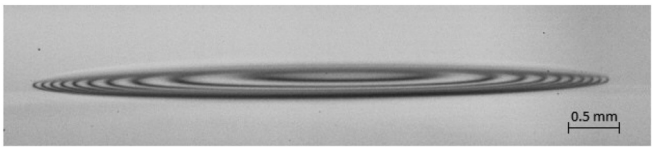

FIG. 2. Drop seen from the side, approximately 2 s after impact. Temperature is 2.5 K. Interference lines show the changing thickness of the drop and are visible due to the slight angle of the imaging system.

per fringe δh (light to light or dark to dark). This thickness δh can be calculated using Eq. (1), with light wavelength λ, helium index of refraction $n_{\text{film}} = 1.03$, and incident angle θ_{inc}. These interference lines can be used to determine the drop topography and dynamic contact angle as discussed in the next section.

$$\delta h = \frac{\lambda}{2\sqrt{n_{\text{film}}^2 - \sin^2\theta_{\text{inc}}}}. \tag{1}$$

III. THERMAL EFFECTS

Drop duration was measured from the time of impact to the total disappearance of the drop. Initial experiments showed that the drop duration varied over a range from 1 to 15 min and seemed to depend on subtle variations in the thermal environment. To investigate this effect systematically, excess power was intentionally injected into the sapphire substrate using a 50 ohm heater epoxied to the side of the sapphire substrate; the very high thermal conductivity of sapphire at low temperature ensured that heat was distributed almost instantly through the substrate with minimal thermal gradients remaining. It became apparent that the normal drop duration was highly sensitive to heat input. Figure 3 shows drop lifetimes as a function of power inserted into the substrate for various temperatures. Unlike superfluid drops (which are discussed in a separate recent publication [16]), the normal helium drops were strongly affected by the heat input, with power inputs as low as 15 μW having an effect on the total drop duration.

The sensitivity of the normal helium drop duration to heat input indicates evaporation as the controlling factor. The candidates for the driving force for evaporation are the Laplace pressure ($\sigma_{\text{lv}}h/R^2$), where h is the thickness of the drop, and the gravitational pressure difference in the vapor from the bottom of the cell ($mgHP_{\text{sat}}/k_bT$), where H is the height of the substrate above the bulk liquid bath, and m is the mass of a helium atom, P_{sat} is the saturated vapor pressure, and k_b is Boltzmann's constant. Assuming the local vapor pressure near the drop is lower than the saturated vapor pressure at the cell temperature T by an amount $\Delta P = \rho_v gH$ where the vapor density $\rho_v = mP_{\text{sat}}(T)/(k_bT)$ implies an inward flux from the vapor into the drop $\dot{N}_{\text{in}}$ with

$$\dot{N}_{\text{in}} = \frac{(P_{\text{sat}}(T) - \rho_v gH)}{k_bT}\sqrt{\frac{3k_bT}{m}}. \tag{2}$$

If the temperature of the drop is T_d, then there is an outward flux from the drop $\dot{N}_{\text{out}}$ given by

$$\dot{N}_{\text{out}} = \frac{(P_{\text{sat}}(T_d) + 2\sigma_{\text{lv}}h/R^2)}{kT}\sqrt{\frac{3k_bT}{m}}. \tag{3}$$

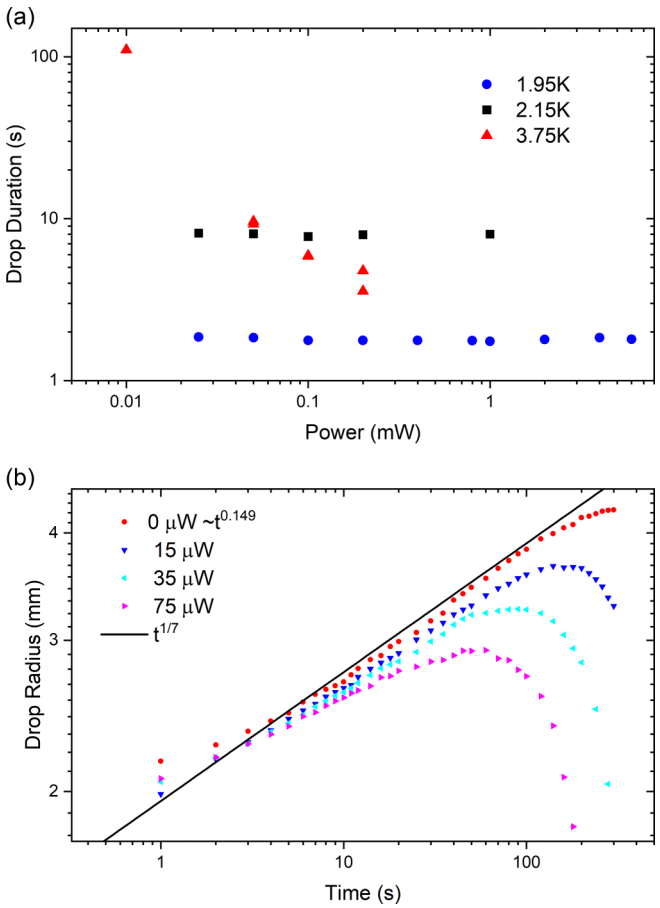

FIG. 3. Effect of heat input on drop lifetime and evolution. Power is applied to the sapphire substrate via an ohmic heater epoxied to the side. (a) Drop duration as a function of heat input for various temperatures. At low temperatures, superfluid drops, shown in blue, have short lifetimes that are independent of heater power. Superfluid drops near T_λ, shown in black, have a longer lifetime, which is nevertheless independent of power. The lifetime of drops in the normal state, shown in red, ranges from ≈300–1000 s at nominally zero power to a few seconds with 0.1 mW of power. (b) Drop spreading radius as a function of time for several values of input power. The radius grows roughly proportional to $t^{1/7}$ until evaporation dominates and the drop starts to shrink. Microwatts of power were sufficient to noticeably increase the evaporation rate.

Assuming isothermal conditions (i.e., $T = T_d$), the net flux out of the drop for isothermal conditions $\dot{N}_{\rm iso}$ is

$$\dot{N}_{\rm iso} = \left(\rho_v g H + \frac{2\sigma_{\rm lv} h}{R^2}\right)\sqrt{\frac{3}{k_b T m}}. \tag{4}$$

For a typical drop at 2.5 K with a $R \approx 0.005$ m, $h \approx 10^{-5}$ m, and $H \approx 0.01$ m, this flux would evaporate the drop in a fraction of a second, which is much shorter than the observed lifetime. Isothermal conditions are not realistic, however, because the outward flux of atoms generates a heat flux $\dot{Q}_{\rm evap} = (\dot{N}_{\rm in} - \dot{N}_{\rm out})\, h_v$, where h_v is the latent heat of vaporization. This heat flux cools the drop, which lowers the vapor pressure and reduces the evaporation rate. In thermal steady state, the temperature of the liquid drop is determined by a balance of the heat flux due to evaporation at the liquid-vapor interface and the steady-state heat flux $\dot{Q}_s$ into the drop at the liquid solid interface. The heat flux from the solid is mainly determined by the thermal boundary resistance, or Kapitza resistance R_k, with

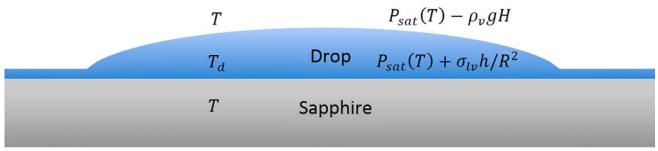

FIG. 4. Schematic diagram of a drop on a sapphire substrate. The sapphire and the vapor above the drop are at cell temperature T. The pressure in the vapor is $P_{\rm sat}(T)$ at the bulk liquid-vapor interface, which is a distance $H \approx 1$ cm below the drop; the vapor pressure above the drop is lower than $P_{\rm sat}(T)$ by an amount $\rho_v g H$. The pressure in the drop is larger than $P_{\rm sat}(T)$ due to the Laplace pressure $\sigma_{\rm lv} H/R^2$. These pressure differences drive an evaporative flux out of the drop, which lowers the drop temperature T_d.

$$\dot{Q}_s = \frac{T_d - T}{R_k}. \tag{5}$$

The Kapitza resistance at a sapphire-helium interface has typical values of $R_k \approx 4 \times 10^{-4}/T^3$ m^{2}K/W [18]; the thermal resistance of the drop itself is negligible compared to the boundary resistance, so the drop can be considered isothermal. In steady state, $\dot{Q}_{\rm evap} = \dot{Q}_{\rm sub}$ (with substrate heat flux $\dot{Q}_{\rm sub}$), which provides an equation for T_d. The calculation yields a perhaps surprisingly small value of $\Delta T = T - T_d \approx 10^{-5}$K. The nonisothermal number flux $\dot{N}_{\rm noniso}$ in this case is

$$\dot{N}_{\rm noniso} = \left(\rho_v g H + \frac{\sigma_{\rm lv} h}{R^2} - \Delta T \frac{dP_{\rm sat}}{dT}\right)\sqrt{\frac{3}{k_b T m}}, \tag{6}$$

where $dP_{\rm sat}/dT$ is the slope of the vapor pressure curve, with a typical value ≈10^4 Pa/K in our case. Substituting a value of the steady state value $\Delta T = 10^{-5}$ K into Eq. (6) yields a flux which would require ≈10^6 s to evaporate the drop, which is much longer than is observed. The large value of $dP_{\rm sat}/dT$ implies, however, that the drop lifetime is very sensitive to the value of ΔT, and nanokelvin deviations from the nominal steady-state value results in drop lifetimes in the range of 10^2–10^3 s that we observe. Figure 4 shows a schematic diagram of a drop on a sapphire substrate.

IV. SPREADING DYNAMICS

A. Experimental results

The impact and spreading of a drop on a surface can be divided into two stages [19,20]. In the initial stage, the kinetic energy of the drop is dissipated as the drop footprint expands to about three times the diameter of the original drop. In this regime, the radius of the position of the contact line at R grows as $t^{1/2}$. In helium with impact velocities of ∼1 m/s, this phase of spreading is completed in less than 100 ms. The short-time dynamics are essentially independent of temperature and the state (superfluid or normal) of the helium and will not be discussed further here. After a quiescent period of a few seconds, the drop continues to spread with a slow creeping flow which is often characterized by a power law $R(t) \sim t^\alpha$, with α in

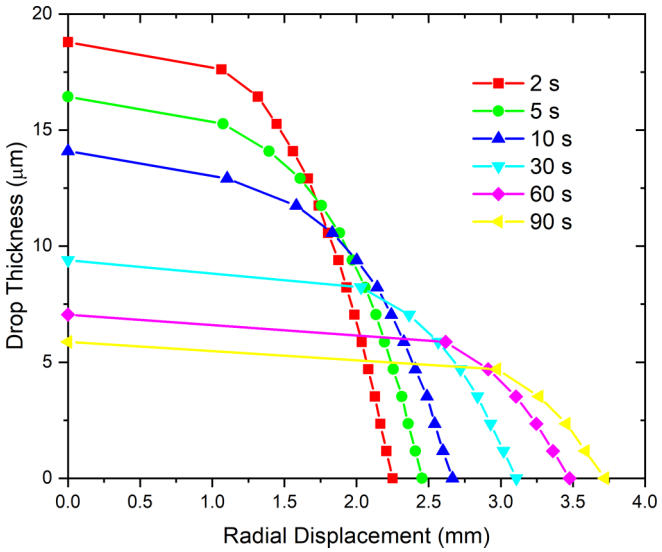

FIG. 5. Drop profile constructed from the interference patterns as a function of time. The horizontal and vertical scales differ by almost a factor of 1000, so the physical drops are exceedingly flat.

the range 0.1–0.15. Because our experiments take place at saturated vapor pressure, the flow occurs over a preexisting film 20–40 nm thick. Although helium completely wets the substrate and the viscosity of ^{4}He is very low ($\sim 3 \times 10^{-6}$ Pa s), a drop deposited on the substrate has a clearly visible contact line that persists throughout its lifecycle as it expands and then eventually retracts due to evaporation.

Both the position of the contact line and the height profile of the spreading drop can be determined by analyzing interferometric images such as those shown in Fig. 2. For a red LED with an optical bandpass filter centered at 632 nm, each fringe in the side view represents a 1167 nm change in drop height. Figure 5 shows the drop profiles for several times, reconstructed from the interference fringes. The macroscopic contact angle calculated from the profile is initially $\sim 1.5^\circ$ and approaches 0.4° at long times.

The radius of the drop footprint as a function of time as deduced from these images is shown in Fig. 6. The best-fit power law for the data in the range 4 s $< t <$ 140 s (to avoid the initial transient and the effects of evaporation at long times) yields $R(t) \sim t^{0.149 \pm 0.002}$.

As described below in the Appendix, various models and assumptions lead to power laws with exponents such as 1/10, 1/8, or 1/7, and experimentally distinguishing among these is a delicate task. One measure of the quality of the fit is χ^2, the sum of the squares of the residuals normalized by the square of the uncertainty (estimated to be 0.02 mm) as a function of the exponent α with $R(t) \sim t^\alpha$. The minimum at $\alpha = 0.149$ is very close to 1/7=0.143, and the residuals for $\alpha = 1/10$ or 1/8 are more than an order of magnitude higher. A plot of χ^2 as a function of α is shown in Fig. 7. An alternative way to represent the data is a model with the functional form $R \sim A(t + t_0)^{(1/n)}$, which is proposed in reference [9]. For gravity driven flow, their analysis suggests that $n = 7$ is valid in a crossover regime between $n = 10$ for drops smaller than the capillary length and $n = 8$ for large drops, but their data using

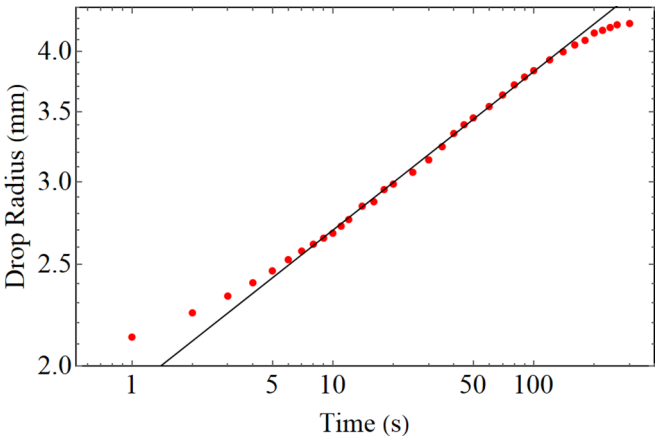

FIG. 6. Drop radius as a function of time for drops at $T = 2.5$ K. The best-fit spreading exponent of 0.149 ± 0.002 using the data with 4 s $< t <$ 140 s is shown as the black line. The best-fit exponent is slightly greater than $1/7 = 0.143$.

PDMS shows no region over which $n = 7$ is applicable [21]. The best-fit parameters for their functional form applied to our data yield $n = 6.27$ and $t_0 = 1.35$.

B. Discussion

The spreading flow of a drop is driven by the gravitational potential energy due to the excess thickness and the excess surface energy of the drop, while viscous forces retard the flow. There are two standard ways of quantitatively analyzing the balance between these forces. One is based on solving approximations to the hydrodynamic equations of motion (expressed as a PDE), while the other equates the rate of change of potential energy to the rate of dissipation (expressed as an ODE). We have used both techniques to model the spreading of drops in our system which is somewhat unusual because spreading takes place at the saturated vapor pressure.

When the thickness of the spreading drop is small compared to its lateral extent, the spreading dynamics can be described by the lubrication approximation, which can be written in terms of a partial differential equation for the time evolution of the drop height $h(r, t)$ as a function of the radial coordinate r and time. The conservation of mass

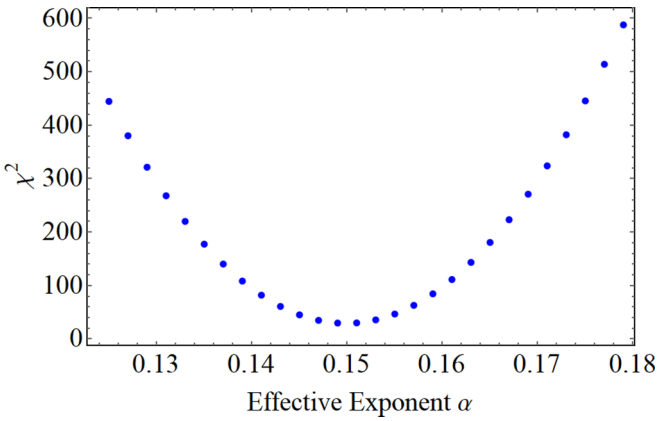

FIG. 7. Plot of χ^2 for fits of the form $R(t) \sim t^\alpha$ to the data of Fig. 6 as a function of α.

for an axisymmetric drop can be expressed as $\partial h/\partial t = \nabla \cdot [h(r,t)v(r,t)]$, where $v(r,t)$ is the fluid velocity in the radial direction averaged over the height of the drop. In keeping with the lubrication approximation, the inertial terms are neglected in the Navier-Stokes equations, so there is a balance between the pressure gradient $\nabla P(r)$ and viscosity, with $\nabla P(r) = \eta \nabla^2 v(r,t)$. The pressure is the sum of a Laplace pressure term proportional to $\sigma_{\rm lv}\nabla^2 h(r,t)$ and a gravitational term proportional to $\rho\, g\, h(r,t)$. The equation of motion for the drop profile $h(r,t)$ is

$$\frac{\partial h}{\partial t} = \frac{1}{3\eta}\{\nabla \cdot [h^3 \nabla(\rho g h - \sigma_{\rm lv}\nabla^2 h)]\}. \tag{7}$$

If only one driving term of this equation is important (i.e., if either $\sigma_{\rm lv}$ or g can be neglected), then self-similar solutions can be constructed [22,23] using the standard ansatz $h(r,t) \sim t^{-\gamma/\beta} f(rt^{-1/\beta})$, where α and β are constants. The contact line corresponds to a point at which $f = 0$. If the contact line is at r_1 at time t_1, then at time t the contact line will move to $r = Ct^{1/\beta}$, where $C = r_1\, t_1^{-1/\beta}$, so the scaling ansatz implies a power law for the time evolution of the drop radius with exponent $1/\beta$. For the curvature-driven flow, Eq. (7) provides one relation between β and γ, $\gamma = (\beta - 4)/3$, and mass conservation in the form

$$\int h(r,t) 2\pi r dr = \text{const} \tag{8}$$

requires $\gamma = 2$, which uniquely determines $\beta = 10$, which is the conventional Tanner's law result. A similar analysis for purely gravity-driven flow yields $\beta = 8$.

If both terms are retained in Eq. (7), then there are no strictly self-similar solutions. A naive estimate of the relative size of the terms assumes that if the typical height is H and the radial length scale is R_c, the gravitational term is of order $\rho g H$ while the surface tension term is of order $\sigma_{\rm lv} H/R_c^2$. This leads to the somewhat counterintuitive conclusion that gravity becomes the dominant term when the drop footprint becomes large and the thickness is small. This estimate is valid for spherical cap drops, but not for the pancake drops we see in our experiments. An experiment which shows the crossover between $t^{1/10}$ behavior at short times and $t^{1/8}$ at long times when gravity dominates is described in Ref. [8].

Although the complete form of Eq. (7) is analytically intractable, some insight can be obtained from direct numerical solutions. The axially symmetric version was put into nondimensional form using the capillary length L_c as the length scale and $\eta/(g\rho\sigma_{\rm lv})$ as the timescale. The nondimensional equations were solved with an initial condition of a Gaussian or hyperbolic tangent shaped drop of width 1 and height 0.5 in reduced units. Using the lubrication approximation to propagate the contact line into a completely dry surface has well known numerical instabilities [24], so the initial condition included a thin film of liquid (~0.001 of the initial drop thickness) that covered the entire solid surface. Typical results are shown in Fig. 8. The initial drop shape quickly evolves into a very flat pancake shape with noticeable curvature only in a region near the contact line which is one capillary length long; these features correspond to what is observed in the experiments, as shown in Fig. 6. Plots of the characteristic radial scale of the pancake as a function of time yields respectable

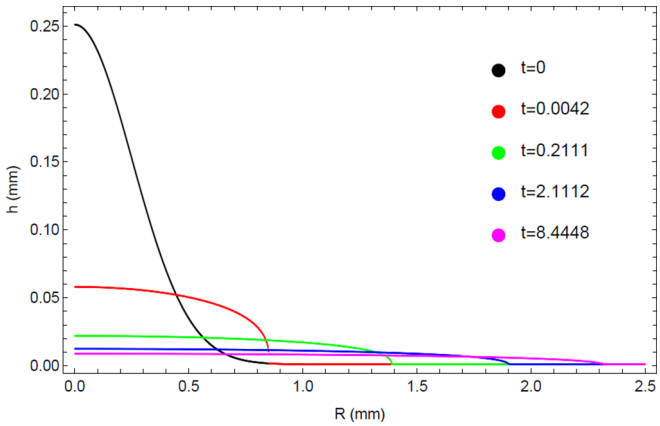

FIG. 8. Numerical solutions for the evolution of the drop profile, showing the drop height in mm as a function of the footprint radius R in mm for various values of the the time t in seconds.

power laws, but the value of the exponent varied by about ±10% depending on the initial shape and the background film thickness, so we were unable to definitively establish the asymptotic behavior of Eq. (8) from the numerical solutions.

Another approach to the determination of the asymptotic spreading law is to invoke the principle that the rate of decrease of the potential energy of the drop which drives spreading must be balanced by dissipation. In particular, the dynamics of spreading is controlled by a balance between the rate of decrease of the gravitational and excess surface energy and viscous dissipation in the bulk flow or dissipative processes at the contact line, together with the constraint of constant volume and the assumption of complete wetting. Using essentially dimensional estimates of the various quantities, a differential equation for the drop footprint radius $R(t)$ can be constructed with asymptotic solutions of the form $R \approx t^{\alpha}$. The numerical value of α depends on the choice of drop geometry and the dominant source of spreading energy and dissipation. The dominant terms in the balance may change as the drop thins, so there are typically several power-law regimes with crossover regions between them. The disk and cone are simple self-similar representative shapes for which the energy and dissipation integrals can be done in closed form. The disk geometry is especially simple and captures most of the physical features of the drops in our experiments, in particular the localization of the excess surface near the contact line. The analysis for the disk leads to a power-law exponent $\alpha = 1/7$, in good agreement with the the value we observe. For completeness, a similar analysis for cone and pancake shaped drops and an alternative dissipation mechanism is presented in the Appendix. In the following discussion, the subscripts may be identified thus: d for disk, s for surface, g for gravity, c for crossover or cone, and p for pancake.

The disk is characterized by a thickness $h(t)$ and a radius $R(t)$. The volume Ω_d is

$$\Omega_d = \pi R(t)^2 h(t). \tag{9}$$

We are interested here in the spreading of a drop over an existing thin film of fluid which nevertheless has bulk-like surface properties, so the difference in surface energy between an equilibrium flat film and a disk-shaped drop is due only to

the surface area of the curved vertical edge, which is

$$E_{\rm ds} = \sigma_{\rm lv} 2\pi R(t)\, h(t) = \frac{2\sigma_{\rm lv}\Omega_d}{R(t)}, \tag{10}$$

where Eq. (9) has been used to eliminate $h(t)$. Similarly, the gravitational potential energy is

$$E_{\rm dg} = \int_0^{h(t)} \rho g z \pi R(t)^2\, dz = \frac{\rho g \Omega_d^2}{2\pi R(t)^2}. \tag{11}$$

A comparison of Eqs. (10) and (11) shows that surface energy is the dominant effect in the limit of large $R(t)$. It is important to note that this ordering of $E_{\rm ds} > E_{\rm dg}$ is the opposite of the the conventional analysis of the lubrication Eq. (7) and for the cone shaped drops discussed below, both of which lead to an $R(t) \sim t^{1/8}$ asymptotic behavior. The volume density of viscous dissipation is $\eta \nabla U^2$, which, in the lubrication approximation, reduces to $\eta(\partial U/\partial z)^2$, where U is the flow velocity. We further assume that $U = 0$ at $z = 0$ and $U = \dot{R}(t)$ at the vapor interface $z = h(t)$, where $\dot{R}(t)$ is the velocity of the contact line. An estimate for the total power dissipated by flow in the disk is

$$\dot{E}_{\rm disk} = \int \eta \left[\frac{\dot{R}(t)}{h(t)}\right]^2 dV = \frac{\eta\, \pi^2 R(t)^4 \dot{R}(t)^2}{\Omega_d}. \tag{12}$$

Equating the rate of change of surface energy to the viscous dissipation yields a differential equation for the contact line velocity $\dot{R}_{\rm ds}(t)$ driven by surface tension in the disk:

$$\dot{R}_{\rm ds}(t) = \frac{2\sigma_{\rm lv}\Omega_d^2}{\pi^2 \eta R_{\rm ds}(t)^6} \Rightarrow R_{\rm ds}(t) \approx \left(\frac{\sigma_{\rm lv}\,\Omega_d^2}{\eta}\right)^{1/7} t^{1/7}. \tag{13}$$

A similar analysis for the gravitational energy yields

$$\dot{R}_{\rm dg}(t) = \frac{\rho g \Omega_d^3}{\pi^3 \eta R_{\rm dg}(t)^7} \Rightarrow R_{\rm dg}(t) \approx \left(\frac{\rho\, g\, \Omega_d^3}{\eta}\right)^{1/8} t^{1/8}. \tag{14}$$

The crossover between these two power laws is determined by equating the rate of change of the surface energy and the gravitational energy $\dot{E}_{\rm ds} = \dot{E}_{\rm dg}$, so the crossover value of $R(t) = R_{\rm dc}$ is

$$R_{\rm dc} = \frac{g\rho\Omega_d}{2\pi\sigma_{\rm lv}}. \tag{15}$$

The crossover value depends on the volume of the drop; for the helium drops in our experiments, $R_{\rm dc}$ is a fraction of a millimeter, so we expect to always observe the surface energy driven result from Eq. (13) with $R(t) \sim t^{1/7}$.

V. CONCLUSION

We have used video imaging and interferometry to study spreading of ^{4}He drops in the normal state. Spreading in this system differs from many previous spreading experiments because spreading takes place in a single-component system at the saturated vapor pressure, so the fluid drop is always at its boiling point. In this single-component system at saturated vapor pressure, the drop does not spread onto a solid substrate, but rather onto a pre-existing thin adsorbed liquid film. Despite the low viscosity, high wettability, and low optical index of liquid helium, there is an easily observable contact line that moves via a creeping flow with a contact angle of approximately one degree. Even at the saturated vapor pressure, drops are always out of equilibrium because of the curvature and the height difference from the bulk liquid, so drops always have a finite lifetime, which imposes an intrinsic limit on the observations of spreading dynamics. The lifetime of the drop is determined by a delicate balance between cooling due to evaporation and heat transport from the solid, and microkelvin temperature variations cause large changes in the lifetime. During the spreading process, the growth of the footprint radius of the drop can be described by a power law with $R(t) \sim t^{0.149}$. The exponent is very close to $1/7$, but experimentally distinguishable from $1/8$, the conventional result for gravity-driven spreading for a large drop [21]. A simple model which balances surface energy near the contact line against bulk viscous dissipation leads to an exponent of $1/7$.

ACKNOWLEDGMENTS

This research was supported by King Abdullah University of Science and Technology (KAUST) under Grant No. URF/1/2621-01-01.

APPENDIX

Balancing the rate of decrease of potential energy to the dissipation rate in the flow yields an asymptotic growth law for axisymmetric drops of the form $R(t) \sim t^{\alpha}$. The value of α depends on the geometry of the drop and the assumptions about the various energy terms, in particular how each term scales with R at constant volume. We argue above that a simple disk geometry captures the essential physical features of our pancake drops; we include here a similar analysis for other geometries and dissipation mechanisms for completeness and to make contact with previous similar discussions [9,25].

1. Cone Geometry

The cone is characterized by a height $h(t)$ and a radius $R(t)$. In contrast to the disk, the cone has a contact angle $\theta_c \sim h[t]/R[t]$ that varies as the drop spreads. The volume Ω_c is

$$\Omega_c = \pi h(t) R(t)^2/3. \tag{A1}$$

The excess surface energy which drives spreading is proportional to the difference between the area of the base and the area of the upper curved surface of the cone:

$$E_{\rm cs} = \sigma_{\rm lv}\left(\pi R(t)^2 \sqrt{\frac{h(t)^2}{R(t)^2} + 1} - \pi R(t)^2\right) \approx \frac{9\sigma_{\rm lv}\Omega_c^2}{2\pi R(t)^4}. \tag{A2}$$

The gravitational energy is

$$E_{\rm cg} = \int_0^{h(t)} \rho g z \pi \left(R(t) - \frac{z R(t)}{h(t)}\right)^2 dz = \frac{3g\rho\Omega_c^2}{4\pi R(t)^2}. \tag{A3}$$

Comparing Eqs. (A2) and (A3), we expect the gravitational term to dominate at large $R(t)$. Assuming again that the velocity varies from zero at $z = 0$ to $\dot{R}(t)$ at the vapor interface,

the volume density of dissipation is

$$\frac{\eta \dot{R}(t)^2}{h(t)^2\left(1-\frac{r}{R(t)}\right)^2}. \tag{A4}$$

The integral of the dissipation has a well-known singularity at the corner of the wedge formed by the contact line due to the divergence of the velocity gradient. The standard cure is to introduce a microscopic cutoff length ϵ,

$$\dot{E}_{\rm cone} = \int_0^{R(t)-\epsilon}\int_0^{h(t)\left(1-\frac{r}{R(t)}\right)} \frac{2\pi r\eta \dot{R}(t)^2}{h(t)^2\left[1-\frac{r}{R(t)}\right]^2} dz dr \sim \frac{2\pi^2 \eta L_f R(t)^4 \dot{R}(t)^2}{3\Omega_c}, \tag{A5}$$

and the result can be expressed in terms of a logarithmic factor $Lf \sim \mathcal{O}\{\mathrm{Log}[\epsilon/R(t)]\}$. Equating the rate of change of surface energy $E_{\rm cs}$ to the viscous dissipation yields an equation for the contact line velocity $\dot{R}_{\rm cs}(t)$ driven by surface tension in the cone:

$$\dot{R}_{\rm cs}(t) = \frac{27\sigma_{\rm lv}\Omega_c^3}{\pi^3 \eta L_f R_{\rm cs}(t)^9} \Rightarrow R_{\rm cs}(t) \approx \left(\frac{\sigma_{\rm lv}\,\Omega_c^3}{Lf\,\eta}\right)^{1/10} t^{1/10}. \tag{A6}$$

The classical Tanner's law which balances surface energy against viscous dissipation in a spherical cap yields the same $1/10$ exponent as above; the slight difference in the curvature does not affect the asymptotic spreading law.

Repeating the analysis for the gravitational energy yields

$$\dot{R}_{\rm cg}(t) = \frac{9g\rho\Omega_c^3}{4\pi^3 \eta L_f R(t)^7} \Rightarrow R_{\rm cg}(t) \approx \left(\frac{\rho\, g\,\Omega_c^3}{L_f\,\eta}\right)^{1/8} t^{1/8}. \tag{A7}$$

The crossover between these two power laws is determined by equating the rate of change of the surface energy and the gravitational energy $\dot{E}_{\rm cs} = \dot{E}_{cg}$, so the crossover value of $R(t) = R_{\rm cc}$ is

$$R_{\rm cc} = \frac{2\sqrt{3\sigma_{\rm lv}}}{\sqrt{g\,\rho}}, \tag{A8}$$

which is the capillary length, to within a numerical factor. For our helium drops, $R_{\rm cc} \sim 1$ mm and is independent of volume, so for larger conical drops, the spreading law will be determined by the gravity driven exponent of $1/8$.

2. Pancake

A pancake drop can be regarded as a combination of a disk-shaped central portion with an end section with a contact line region similar to the cone. The pancake drop is characterized by a height $h(t)$, a disk radius $R(t)$, and a capillary length L_c which is the width of the region in which the drop thins from $h(t)$ to zero at the contact line; in helium throughout our temperature range, the capillary length is approximately half a millimeter. Because of this additional length scale in the problem, some of the integrals cannot be done in closed form, so the results are reported to first order in L_c. The pancake volume is

$$\Omega_p = \pi\, L_c\, h(t) R(t) + \pi h(t) R(t)^2. \tag{A9}$$

The excess surface energy which drives spreading is due to the area of the nonhorizontal section of the drop near the contact line:

$$E_{\rm ps} = \frac{2\sigma_{\rm lv}\,\Omega_p}{R(t)} - \frac{L_c\,\sigma_{\rm lv}\Omega_p}{R(t)^2}. \tag{A10}$$

The gravitational energy is

$$E_{\rm pg} = \frac{\rho g \Omega_p^2}{2\pi R(t)^2} - \frac{2g\,L_c\,\rho\Omega_p^2}{3\pi R(t)^3}. \tag{A11}$$

Comparison of Eqs. (A10) and (A11) suggest that the surface term will dominate for large drops. Equating the rate of change of the surface energy and the gravitational energy $\dot{E}_{\rm ps} = \dot{E}_{\rm pg}$, the crossover value of $R(t) = R_{\rm pc}$ is simply $R_{\rm pc} = 2L_c$, which is about 1 mm for our drops. For larger pancake drops, the main driving force for spreading is surface tension. The viscous dissipation in the pancake drop consists of two terms: one has the same form as dissipation in the disk, and the other is similar to the dissipation in the corner of the cone,including the logarithmic factor L_f, but since the integral extends over a length L_c rather than $R(t)$, the result is proportional to L_c. The total dissipation is

$$\dot{E}_{\rm pan} = \frac{\pi^2\eta\, L_c\,(1-2L_f) R(t)^3 R'(t)^2}{\Omega_p} + \frac{\pi^2\eta R(t)^4 \dot{R}(t)^2}{\Omega_p}. \tag{A12}$$

Equating the rate of change of surface energy $E_{\rm ps}$ to the viscous dissipation yields an equation for the contact line velocity $\dot{R}_{\rm ps}(t)$ driven by surface tension in the pancake drop:

$$\dot{R}_{\rm ps}(t) = \frac{2\Omega_p^2[L_c\,\sigma - \sigma R(t)]}{\pi^2\eta R(t)^6[2L_c\,L_f - L_c - R(t)]} \approx \frac{2\sigma\,\Omega_p^2}{\pi^2\eta R(t)^6} + \frac{4L_c(L_f\,\sigma - \sigma)\Omega_p^2}{\pi^2\eta R(t)^7}. \tag{A13}$$

To zeroth order in L_c, the asymptotically large $R(t)$ pancake result is identical to the disk result and leads to an exponent of $1/7$; for smaller drops, there is a correction term $R(t) \sim \mathcal{O}(t^{1/8})$.

3. Molecular Kinetic Dissipation

An alternate approach to contact line spreading dynamics is called molecular kinetic theory [11,26,27]. The model ignores dissipation in the bulk fluid and focuses on forces and dissipation at the contact line. The basic idea is that a contact line with an external force F can be pinned by local inhomogeneities in the substrate, but the the contact line can make thermally activated jumps of length Δx at a rate ν. If the jump is in the direction of the external force, then the energy goes down by an amount $\Delta E = F\,\Delta x$, and if it makes a transition against the force, the energy goes up by the same amount. The sum of the transitions leads to motion of the contact line with velocity $\dot{R}_{\rm MKT}(t)$ given by

$$\dot{R}_{\rm MKT}(t) = \Delta \mathrm{x}\,\nu\left(e^{\frac{\Delta \mathrm{E}}{k_b T}} - e^{-\frac{\Delta \mathrm{E}}{k_b T}}\right) \approx \frac{2\Delta \mathrm{E}\Delta \mathrm{x}\,\nu}{k_b T} \tag{A14}$$

This expression is presumably valid only near equilibrium. Determining the asymptotic behavior of $R_{\rm MKT}(t)$ requires making assumptions about the $R(t)$ dependence of ΔE, or

equivalently, the force per unit length on the contact line which can be calculated from the $R(t)$ derivative of the surface or gravitational energy for a given drop geometry. For example, for surface-tension-driven spreading of a conical drop, the force per unit length is the derivative at constant volume of the surface energy from Eq. (A6):

$$\dot{R}(t) \sim -\frac{1}{2\pi R(t)}\frac{\partial E_{\rm cs}}{\partial R(t)} \sim \frac{\sigma\Omega_c}{R(t)^6} \Rightarrow R(t) \sim t^{1/7}. \quad \text{(A15)}$$

The $t^{1/7}$ power law for the surface tension driven flow with molecular kinetic friction for a spherical cap drop is well-known [10–12]. The value of the exponent depends crucially, however, on the shape of the drop; for surface tension driven flow for a disk or pancake shaped drop with energy described by Eq. (10), the molecular kinetic theory yields

$$\dot{R}(t) \sim -\frac{1}{2\pi R(t)}\frac{\partial E_{\rm ds}}{\partial R(t)} \sim \frac{\sigma\Omega_d}{R(t)^3} \Rightarrow R(t) \sim t^{1/4}. \quad \text{(A16)}$$

The molecular kinetic $t^{1/4}$ power law for disklike or pancake drops seems to be incompatible with our experimental results.

[1] P. G. Degennes, Wetting—Statics and dynamics, Rev. Mod. Phys. **57**, 827 (1985).

[2] J. Lopez, C. A. Miller, and E. Ruckenstein, Spreading kinetics of liquid-drops on solids, J. Colloid Interface Sci. **56**, 460 (1976).

[3] M. Brenner and A. Bertozzi, Spreading of Droplets on a Solid-Surface, Phys. Rev. Lett. **71**, 593 (1993).

[4] M. J. de Ruijter, M. Charlot, M. Voue, and J. De Coninck, Experimental evidence of several timescales in drop spreading, Langmuir **16**, 2363 (2000).

[5] A. L. Yarin, Drop impact dynamics: Splashing, spreading, receding, bouncing, in *Annual Review of Fluid Mechanics*, Vol. 38 (Annual Reviews, Palo Alto, CA, 2006), pp. 159–192.

[6] L. H. Tanner, Spreading of silicone oil drops on horizontal surfaces, J. Phys. D: Appl. Phys. **12**, 1473 (1979).

[7] D. Bonn, J. Eggers, J. Indekeu, J. Meunier, and E. Rolley, Wetting and spreading, Rev. Mod. Phys. **81**, 739 (2009).

[8] A. M. Cazabat and M. A. C. Stuart, Dynamics of wetting—Effects of surface-roughness, J. Phys. Chem. **90**, 5845 (1986).

[9] F. Brochardwyart, H. Hervet, C. Redon, and F. Rondelez, Spreading of heavy droplets. 1. Theory, J. Colloid Interface Sci. **142**, 518 (1991).

[10] F. T. Dodge, The spreading of liquid droplets on solid-surfaces, J. Colloid Interface Sci. **121**, 154 (1988).

[11] J. De Coninck, M. J. de Ruijter, and M. Voue, Dynamics of wetting, Curr. Opin. Colloid Interface Sci. **6**, 49 (2001).

[12] M. J. de Ruijter, J. De Coninck, and G. Oshanin, Droplet spreading: Partial wetting regime revisited, Langmuir **15**, 2209 (1999).

[13] J. E. Rutledge and P. Taborek, Prewetting Phase-Diagram of He-4 on Cesium, Phys. Rev. Lett. **69**, 937 (1992).

[14] D. Ross, J. E. Rutledge, and P. Taborek, Superfluid droplets on a solid surface, Science **278**, 664 (1997).

[15] A. Prevost, E. Rolley, and C. Guthmann, Dynamics of a helium-4 meniscus on a strongly disordered cesium substrate, Phys. Rev. B **65**, 064517 (2002).

[16] M. L. Wallace, D. Mallin, M. Milgie, A. A. Aguirre-Pablo, K. R. Langley, S. T. Thoroddsen, and P. Taborek, Impact and lifecycle of superfluid helium drops on a solid surface, Phys. Rev. Fluids **5**, 093602 (2020).

[17] M. N. Popescu, G. Oshanin, S. Dietrich, and A. M. Cazabat, Precursor films in wetting phenomena, J. Phys.: Condens. Matter **24**, 243102 (2012).

[18] G. L. Pollack, Kapitza resistance, Rev. Mod. Phys. **41**, 48 (1969).

[19] R. Rioboo, M. Marengo, and C. Tropea, Time evolution of liquid drop impact onto solid, dry surfaces, Exp. Fluids **33**, 112 (2002).

[20] C. Josserand and S. T. Thoroddsen, Drop impact on a solid surface, Annu. Rev. Fluid Mech. **48**, 365 (2016).

[21] C. Redon, F. Brochardwyart, H. Hervet, and F. Rondelez, Spreading of heavy droplets. 2. Experiments, J. Colloid Interface Sci. **149**, 580 (1992).

[22] R. Chebbi, Viscous-gravity spreading of time-varying liquid drop volumes on solid surfaces, J. Colloid Interface Sci. **300**, 688 (2006).

[23] J. A. Diez, R. Gratton, L. P. Thomas, and B. Marino, Laplace pressure-driven drop spreading, Phys. Fluids **6**, 24 (1994).

[24] J. A. Diez and L. Kondic, Computing three-dimensional thin film flows including contact lines, J. Comput. Phys. **183**, 274 (2002).

[25] W. Q. Ren, D. Hu, and W. N. E, Continuum models for the contact line problem, Phys. Fluids **22**, 102103 (2010).

[26] T. D. Blake and J. M. Haynes, Kinetics of liquid/liquid displacement, J. Colloid Interface Sci. **30**, 421 (1969).

[27] D. Seveno, A. Vaillant, R. Rioboo, H. Adao, J. Conti, and J. De Coninck, Dynamics of wetting revisited, Langmuir **25**, 13034 (2009).